

Distinct Proton and Water Reduction Behavior with a Cobalt(III) Electrocatalyst Based on Pentadentate Oximes**

Debashis Basu, Shivnath Mazumder, Xuetao Shi, Richard J. Staples, H. Bernhard Schlegel,* and Cláudio N. Verani*

Abstract: A new pentadentate oxime has been designed to drive the preferential coordination favored by Co^I in catalysts used for proton/water reduction. The ligand incorporates water upon metal coordination and is water soluble. This Co^{III} species is doubly reduced to Co^I and exhibits H^+ reduction activity in the presence of weak acids in MeCN and evolves H_2 upon protonation suggesting that the ligand design increases catalyst effectiveness. Superior catalysis is observed in water with a turnover number (TON) of 5700 over 18 h. However, the catalyst yields Co-based nanoparticles, indicating that the solvent media may dictate the nature of the catalyst.

Generation of H_2 from H^+ or H_2O has driven extensive research as a replacement for nonrenewable fossil fuels.^[1] The use of H^+ involves a $2e^-$ transfer to generate a Co^I species which yields 1 equiv of H_2 . Among well-known examples of H^+ reduction catalysts, Co^{III} glyoxime-based oximes^[2] have been investigated in great detail, in which the catalytic $^{LS}3d^8$ Co^I state seems to favor a five-coordinate environment required for nucleophilic attack on the proton.^[2c,3] However important this 5-coordinate species is, current designs favor untethered axial ligands that dissociate easily, contributing to sluggish electro- and photocatalytic reactivity and degradation of the molecular catalyst.^[4] Ergo, rational ligand design must include pentadentate oximes for the investigation of new catalyst frameworks. Moreover, such ligand design can be useful to address other relevant issues of glyoxime-based systems; 1) the mechanisms of catalyst degradation in acidic media, and 2) the quest for water-soluble systems. Furthermore, conversion of the catalyst into Co-oxide nanoparticles at the surface of the electrode has been reported for glyoximes^[5] and pyridyloximes,^[6] and requires further atten-

tion. The most studied systems for H_2 generation from water^[7] include cobalt complexes of tetra- and pentapyridines^[8] as well as iminopyridines.^[9] We have shown that $[\text{N}_2\text{O}_3]$ ligands support cobalt complexes in catalytic proton reduction.^[10] Adapting this design to pyridine-rich environments yielded water reduction catalysts capable of 7000 turnovers.^[11]

Here we report on a pentadentate N-rich oxime ligand H_2L^1 , its coordination to Co^{II} and water incorporation through one of the imine double bonds to form the water-soluble catalytic species $[\text{Co}^{III}(\text{HL}^1)\text{Cl}]\text{PF}_6$ (**1**), shown in Figure 1. Catalyst **1** presents distinct mechanisms of H_2 generation in acidic organic media and in water.

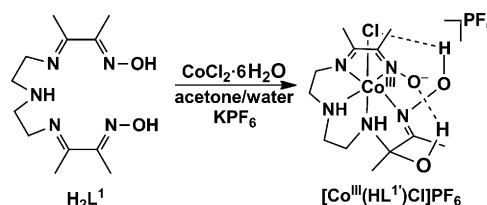


Figure 1. Synthetic scheme of the Co^{III} complex (**1**).

The ligand $\text{H}_2\text{L}^{1[12]}$ contains one secondary amine along with two imine and two oxime nitrogen donor atoms. The redox-active and π -accepting nature of the imine and oxime moieties stabilizes the monovalent cobalt responsible for catalytic activity. Moreover, the pentadentate and macrocyclic nature of H_2L^1 is expected to inhibit the lability of the N atoms. Reaction of the ligand with $\text{CoCl}_2 \cdot 6\text{H}_2\text{O}$ in acetone/water (9:1) yields **1** in which a chloride occupies the sixth position (Figure 1, Scheme S1) and water incorporation was observed through one of the imine bonds.

Comparison between the pentadentate **1** and the tetradentate glyoxime analogue (Figures S2 and S3) confirmed the former as susceptible to water addition; whereas water incorporation in the $[\text{N}_4]$ oxime is detrimental to the conjugated planar ligand framework and unfavorable by ca. 11 kcal mol⁻¹. The decreased electronic communication between the imine moieties in H_2L^1 together with the formation of a strong $\text{OH} \cdots \text{O}$ hydrogen bond of 1.72 Å in the resulting aqua complex make this incorporation favorable by ca. 4 kcal mol⁻¹.

Complex **1** was characterized by multiple spectroscopic and spectrometric methods (Figures S4 and S5), and by elemental analyses. The presence of a PF_6^- counterion was established as a broad IR peak at 832 cm⁻¹. The diamagnetic nature of the $^{LS}3d^6$ **1** was validated by the presence of sharp

[*] D. Basu, Dr. S. Mazumder, X. Shi, Prof. H. B. Schlegel, Prof. C. N. Verani
 Department of Chemistry, Wayne State University
 5101 Cass Ave, Detroit, MI 48202 (USA)
 E-mail: cnverani@chem.wayne.edu
 Homepage: <http://chem.wayne.edu/veranigroup/>
 Dr. R. J. Staples
 Department of Chemistry, Michigan State University
 Lansing, MI 48824 (USA)

[**] This material is based upon work supported by the U.S. Department of Energy, Office of Science, Office of Basic Energy Sciences under award number DE-SC0001907 to C.N.V. and H.B.S., including financial support to D.B. (synthesis & catalysis), S.M. and X.S. (calculations). Dr. Zhi Mei is acknowledged for SEM measurements and Prof. John F. Endicott is acknowledged for critical discussions.

Supporting information for this article is available on the WWW under <http://dx.doi.org/10.1002/anie.201501410>.

peaks in the ^1H NMR spectra. ESI-MS analysis confirmed the presence of the molecular ion species $[\text{Co}^{\text{III}}(\text{HL}^1)\text{Cl}]^+$ with $m/z = 380.0900$ in MeOH.

Structural information (Tables T1 and T2 in the Supporting Information) was gathered from crystals obtained by recrystallization from MeOH/ H_2O (2:1). The structure of **1**, Figure 2, confirmed the distorted octahedral nature of the

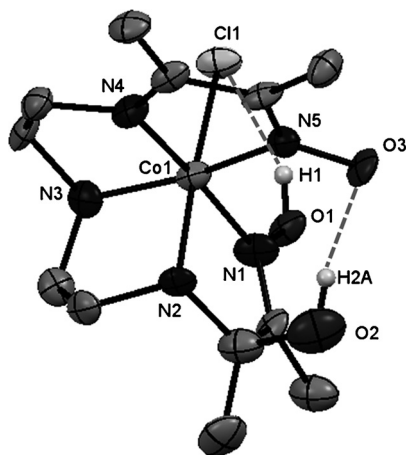


Figure 2. The ORTEP representation of the cation of mononuclear $[\text{Co}^{\text{III}}(\text{HL}^1)(\text{Cl})]\text{PF}_6$ complex (**1**) at 50% probability. Selected bond lengths in Å: Co(1)–N(1) 1.925(7), Co(1)–N(2) 1.949(6), Co(1)–N(3) 1.947(8), Co(1)–N(4) 1.865(6), Co(1)–N(5) 1.894(7), Co(1)–Cl(1) 2.248(2), O(1)–N(1) 1.375(8), O(3)–N(5) 1.304(9). CCDC 1057063 contains the supplementary crystallographic data for this paper. These data can be obtained free of charge from The Cambridge Crystallographic Data Centre via www.ccdc.cam.ac.uk/data_request/cif.

complex with a chlorido ligand occupying the sixth position. Incorporation of H_2O is diagnostic of the newly formed C–O(H) and the lengthening of the C=N bond to C–N from ca. 1.30 to 1.48 Å. Two H-bonding interactions seem to be operative in the stabilization of the molecular structure. The newly incorporated OH forms an H-bond with the formally deprotonated oxime O(3) atom, whereas the second H-bond is formed between the oxime O(1)H and the chloride ligand. This particular orientation of atoms is the most stable thermodynamic configuration, as confirmed by DFT calculations (Figure S3).

Electronic spectroscopic studies were performed in MeCN for the parent $[\text{Co}^{\text{III}}(\text{HL}^1)\text{Cl}]^+$ (**1**) species. The yellowish $^{\text{LS}}3\text{d}^6$ parent species **1** shows an absorption band in the visible region at 441 nm ($\epsilon = 627 \text{ M}^{-1} \text{ cm}^{-1}$) originating from a d–d transition tentatively associated with the $^1\text{T}_{2\text{g}}(\text{I}) \leftarrow ^1\text{A}_{1\text{g}}(\text{D})$ process of an ideal octahedral field (Figure S6, Table T3). Cyclic voltammetry (CV) was performed in MeCN (Figure 3). Three quasi-reversible processes are observed at $-0.75 \text{ V}_{\text{Fc}/\text{Fc}^+}$ ($\Delta E = 0.12 \text{ V}$; $i_{\text{pc}}/i_{\text{pa}} = 1.29$), for the $\text{Co}^{\text{III}}/\text{Co}^{\text{II}}$ couple, $-1.68 \text{ V}_{\text{Fc}/\text{Fc}^+}$ ($\Delta E = 0.10 \text{ V}$; $i_{\text{pc}}/i_{\text{pa}} = 1.5$), for the $\text{Co}^{\text{II}}/\text{Co}^{\text{I}}$ couple, and $-1.86 \text{ V}_{\text{Fc}/\text{Fc}^+}$ ($\Delta E = 0.10 \text{ V}$; $i_{\text{pc}}/i_{\text{pa}} = 1.4$), associated with ligand reduction. The potentials of **1** were recorded in five different solutions and confirmed reproducibility of the data.

Catalytic proton reduction studies were performed in MeCN by CV experiments in the presence of various weak acids such as Et_3NHCl ($\text{p}K_{\text{a}} = 18.7$; Figure S7) and HOAc

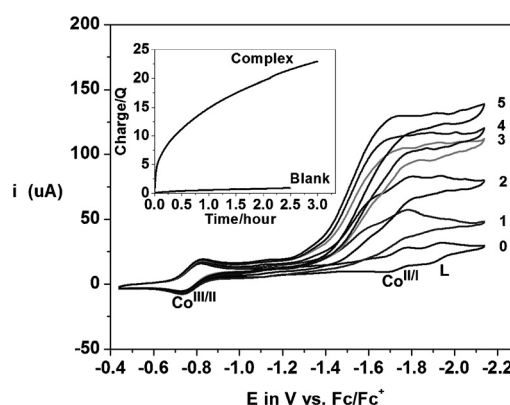


Figure 3. CV experiments for H_2 generation. The numbers 0–5 indicate the equivalents of HOAc used in comparison to **1**. Inset: Charge-versus-time plot for **1** in comparison with an HOAc blank for 3 h during bulk electrolysis.

($\text{p}K_{\text{a}} = 22.3$; Figure 3). The H^+/H_2 catalytic peak was observed close to the second reduction process for these weak acids. Due to our interest in water reduction we focused our attention on the weakest acid, HOAc. The catalytic peak becomes evident at potentials close to $-1.50 \text{ V}_{\text{Fc}/\text{Fc}^+}$ peaking at five equivalents of the acid, with clear formation of a gaseous product. The catalytic current reaches $130 \mu\text{A}$ after addition of five equivalents of acid; an overpotential of 0.24 V was observed after considering the homoconjugation effect.^[13] The fact that a lower overpotential is observed in presence of **1** associated with a higher catalytic current than that of the blank (Figure S8) validates the complex as the catalyst. Controlled potential electrolysis was performed at $-1.7 \text{ V}_{\text{Ag}/\text{AgCl}}$ to confirm the identity of the gaseous product as dihydrogen. Complex **1** consumes more charge than the blank during the bulk-electrolysis experiment (Figure 3 inset), which supports that the complex is responsible for catalysis.

The turnover number (TON) in MeCN for **1** reaches 14.7 after 3 h with a Faradaic efficiency (%F) of 75% in the presence of 100 equivalents of acid. The color of the solution remains unaltered and the corresponding postcatalysis visible spectrum under anaerobic conditions shows peaks at 265 and 325 nm (Figure S9) in excellent agreement with the reduced $3\text{d}^7 \text{Co}^{\text{II}}$ species (Figure S10), suggesting that the molecular catalyst is preserved and no nanoparticles are formed. These results confirm the relevance of the fifth coordination to an axial position of the cobalt ion and suggest a feature to be considered in future ligand design. The DFT-optimized geometries for **1** and its relevant reduced species are summarized in Figure 4. The parent Co^{III} complex displays a pseudo-octahedral geometry with two H-bonds, $\text{OH}\cdots\text{O}$ and $\text{OH}\cdots\text{Cl}$.

A 1 e^- reduction yields a $^{\text{LS}}3\text{d}^7 \text{Co}^{\text{II}}$ complex, in which occupation of an antibonding e_{g}^* -like, Co-based 3d_{z^2} orbital weakens the metal–ligand interactions along the z -axis fostering an increase in the Co–Cl and Co–N bond distances to 2.82 and 2.20 Å, respectively. The $\text{OH}\cdots\text{Cl}$ interaction becomes stronger as the H-bond distance decreases from 2.09 in **1** to 1.98 Å in the Co^{II} species. Dissociation of chloride from the later complex requires 6 kcal mol^{-1} . Reduction of the Co^{II} complex affords the five-coordinate and distorted square

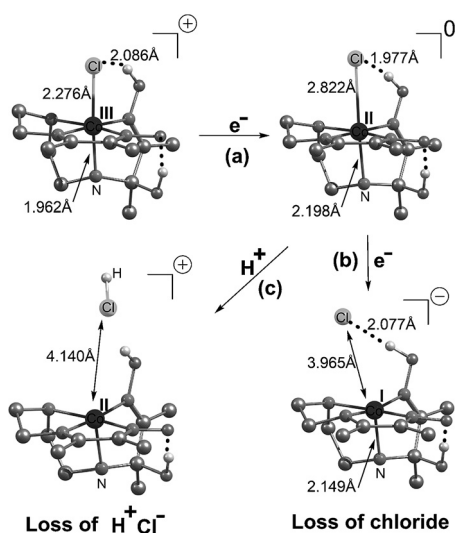


Figure 4. Calculated structures of species electrochemically generated in MeCN: a) $\text{Co}^{\text{III}}/\text{Co}^{\text{II}}$ reduction, b) $\text{Co}^{\text{II}}/\text{Co}^{\text{I}}$ reduction, and c) loss of chloride from the Co^{II} species in the presence of H^+ .

pyramidal Co^{I} species. At ca. 4 Å from the metal center, the Cl^- is no longer part of the coordination sphere. Figure 3 shows an anodic shift of ca. 0.18 V observed upon addition of acid to **1** in MeCN. The electrocatalytic peak was found at potentials close to $-1.50 \text{ V}_{\text{Fc}/\text{Fc}^+}$ whereas the $\text{Co}^{\text{II}}/\text{Co}^{\text{I}}$ process is observed at $-1.68 \text{ V}_{\text{Fc}/\text{Fc}^+}$ in absence of acid. DFT calculations find that in presence of acid the addition of a proton on the Co^{II} species results in the loss of Cl^- as H^+Cl^- giving rise to the five-coordinate cationic Co^{II} complex (Figure 4). The later species can be further reduced to the corresponding Co^{I} complex. The reduction potentials of the $[\text{Co}^{\text{II}}(\text{HL}^{\text{I}})]^+ / [\text{Co}^{\text{I}}(\text{HL}^{\text{I}})]$ and $[\text{Co}^{\text{II}}(\text{HL}^{\text{I}})\text{Cl}] / [\text{Co}^{\text{I}}(\text{HL}^{\text{I}})\text{Cl}]^-$ couples are calculated as -1.65 and $-1.89 \text{ V}_{\text{Fc}/\text{Fc}^+}$, respectively. As an alternative, a proton-coupled electron transfer (PCET) mechanism from $[\text{Co}^{\text{II}}(\text{HL}^{\text{I}})\text{Cl}]$ to Co^{III} hydride $[\text{Co}^{\text{III}}(\text{H})(\text{HL}^{\text{I}})]$ was considered without chloride loss from the Co^{II} complex. The redox potential for the PCET $\text{Co}^{\text{II}}/\text{Co}^{\text{III}}\text{-H}$ couple is calculated^[14] as $-1.55 \text{ V}_{\text{Fc}/\text{Fc}^+}$. The anodic shift calculated by Cl^- loss from the Co^{II} complex is 0.24 V and in better agreement with the experimental 0.18 V, whereas the shift in the potential from the PCET mechanism is 0.34 V and differs by 0.16 V from the experiment.

The DFT-calculated mechanism of H_2 generation by **1** in acidic MeCN is shown in Figure 5. Binding of a proton to the Co^{I} complex results in the $2e^-$ oxidation of the latter giving rise to a $\text{Co}^{\text{III}}\text{-H}$ (Co^{III} hydride) species. The $\text{Co}^{\text{III}}\text{-H}$ complex can be reduced to a more reactive $\text{Co}^{\text{II}}\text{-H}$ species at a potential of $-1.43 \text{ V}_{\text{Fc}/\text{Fc}^+}$. Uptake of another H^+ and generation of H_2 by this $\text{Co}^{\text{II}}\text{-H}$ complex is favorable by 46 kcal mol^{-1} regenerating the five-coordinate Co^{II} complex to restart the cycle. The reaction of H^+ with the $\text{Co}^{\text{II}}\text{-H}$ species is activationless.^[14] Compared to the heterolytic mechanism, homolytic coupling of two $\text{Co}^{\text{II}}\text{-H}$ units is unfavorable by ca. 32 kcal mol^{-1} .

Complex **1** is water soluble due to the presence of various polar groups such as $-\text{NH}$ and $-\text{OH}$. Thus, CV experiments were performed to study the viability of **1** as electrocatalyst

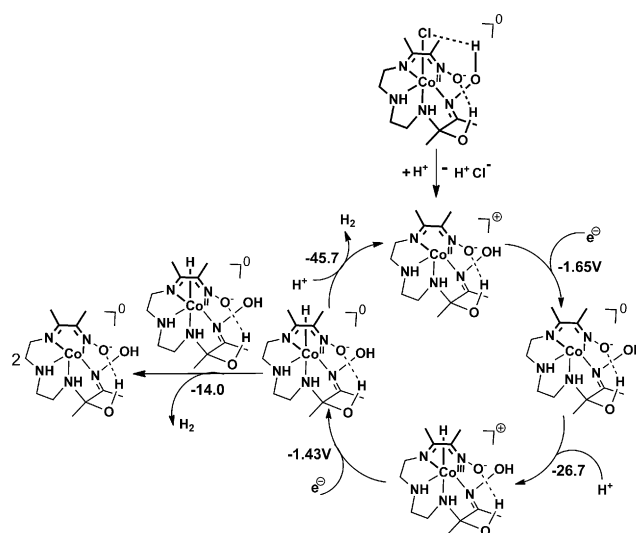


Figure 5. Catalytic mechanism of H_2 generation by **1** in MeCN. Free-energy changes in kcal mol^{-1} .

for the reduction of water at pH 7 in the presence of phosphate buffer using a Hg-pool cell. We observed a peak at $-1.25 \text{ V}_{\text{Ag}/\text{AgCl}}$, which corresponds to the $\text{Co}^{\text{II}}/\text{Co}^{\text{I}}$ process, followed by a sharp increase of current from $-1.30 \text{ V}_{\text{Ag}/\text{AgCl}}$ assigned to the catalytic peak for H_2 evolution. An onset overpotential of 0.65 V was calculated for this system. This result is relevant when compared to the blank experiment in absence of **1** in which H_2 is generated at $-1.90 \text{ V}_{\text{Ag}/\text{AgCl}}$, a much more negative potential (Figure 6). This result validates **1** as

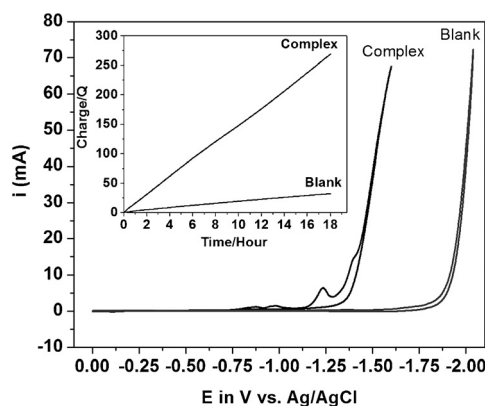


Figure 6. CV experiments for H_2 generation in water/phosphate buffer (pH 7): Blank versus **1** (inset: plot of charge versus time in the bulk electrolysis experiment for **1** at $-1.7 \text{ V}_{\text{Ag}/\text{AgCl}}$ for 18 h).

water-reduction catalyst with a low onset overpotential similar to other water-reduction catalysts.^[7–9] Bulk electrolysis was performed at $-1.7 \text{ V}_{\text{Ag}/\text{AgCl}}$ during 3 h to confirm the presence of H_2 . A TON of 950 was calculated after 3 h with %F of 95%. The activity of the catalyst was assessed by performing an extended controlled potential experiment for 18 h at $-1.7 \text{ V}_{\text{Ag}/\text{AgCl}}$. As indicated in the inset in Figure 6 a linear charge build-up indicative of continued catalysis was observed over time associated with 5680 TONs and %F of 95%. Moreover, a $\text{Co}^{\text{II}}/\text{Co}^{\text{I}}$ process^[7b,8b] found in water at

$-1.25 V_{\text{Ag}/\text{AgCl}}$ ($-1.68 V_{\text{Fc}/\text{Fc}^+}$) supports the formation of a Co^{I} species. Thus, a PCET mechanism does not seem viable under the conditions of our study.

Catalytic parameters are summarized in Table T4. The actual overpotential of this complex was determined by controlled electrolysis at different potentials. The overpotentials were applied over a period of 60 s and altered from 0.45 to 0.95 V to determine the rate of H_2 production (Figure S11) showing increase in charge consumption after 0.65 V consistent with the generation of H_2 bubbles. During the extended bulk electrolysis shown in Figure 6 (inset) an approximate ten times more charge (270 vs. 25 μA) was consumed than in the blank experiment, thus indicating **1** as responsible for catalysis. The UV-visible spectra of the postcatalysis solution was also measured at -1.25 , -1.40 , and $-1.70 V_{\text{Ag}/\text{AgCl}}$ (Figure S12) as a means to probe the resilience of the catalyst. As we observed spectral changes, the nature of the catalytic events was thoroughly investigated. Electrolysis for 1 h at $-1.25 V_{\text{Ag}/\text{AgCl}}$ resulted in some degree of color change from deep to pale yellow with the corresponding intensities of the UV-visible peaks being reduced by ca. 40% (Figure S12a). The near-complete disappearance of the UV-visible bands at ca. 95% was observed after 1 h electrolysis at -1.40 and $-1.70 V_{\text{Ag}/\text{AgCl}}$ (Figure S12b,c). As the catalytic activity was maintained, this was suggestive of the formation of nanoparticles.^[5] This hypothesis was probed by performing a “rinse” experiment in water at pH 7: A glassy carbon electrode was used in water in the presence of **1** and scanned to $-1.70 V_{\text{Ag}/\text{AgCl}}$ followed by extensive rinsing and dipping into a freshly prepared solution with no complex. A catalytic peak appeared around $-1.15 V_{\text{Ag}/\text{AgCl}}$, thus before the potential peak observed for the bare electrode (Figure S13), and implied that nanoparticle deposition on the surface of the electrode enables water reduction. Further confirmation was obtained by scanning electron microscopy analyses of a graphite foil working electrode before and after bulk electrolysis in water at -1.45 and $-1.70 V_{\text{Ag}/\text{AgCl}}$. The SEM images shown in Figure 7 confirm the formation of cobalt-based nanoparticles

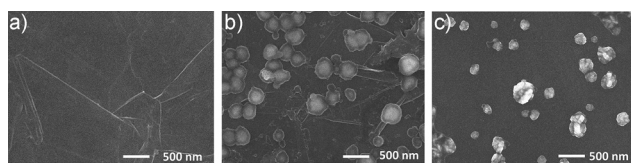


Figure 7. SEM images of the graphite foil electrode: a) bare, before electrolysis; with deposited particles after bulk electrolysis at b) $-1.45 V_{\text{Ag}/\text{AgCl}}$ and c) $-1.70 V_{\text{Ag}/\text{AgCl}}$. Scale bars = 500 nm.

with a size distribution between 80–300 nm. Similar observations were described in recent studies.^[5,6] Although the composition of these nanoparticles is unknown, the ligand architecture was proposed to be crucial in the nanoparticle activity.^[15]

To gain more insight into the catalyst decomposition process in water, we have considered the hydrolysis of the imine bonds in the Co^{II} and Co^{I} complexes. The later species is more susceptible to water incorporation^[5] (Figures S14 and

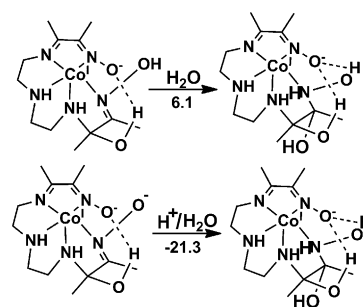


Figure 8. Possible pathways for the decomposition of the catalyst in water. Free-energy changes in kcal mol^{-1} .

S15). Addition of a water molecule to an isolated imine bond of the Co^{I} complex is energetically uphill by only 6 kcal mol^{-1} (Figure 8) and is feasible in the presence of a large excess of water. Moreover, the acid strength of the $\text{C}=\text{N}(\text{OH})$ function is expected to be greater in more polar aqueous solvent than in MeCN and as a result, a greater fraction of the deprotonated form $\text{C}=\text{N}(\text{O}^-)$ is present in water (Figure S16). Incorporation of a water molecule into the imine bond of this deprotonated ligand backbone is significantly favorable by ca. 21 kcal mol^{-1} (Figure 8). These results indicate a number of possible pathways that can lead to catalyst decomposition and subsequent nanoparticle formation in water and are in agreement with a recent study^[16] of the formation of Co-nanoparticle H_2 -evolution catalyst by the use of an inorganic cobalt salt in neutral water. A detailed study of the mechanism of catalyst decomposition and nanoparticle formation is currently underway.

In conclusion, a new five-coordinate proton reduction catalyst, **1**, was obtained. Water incorporation was observed through one of the imine bonds and H-bonding interactions stabilize the resulting structure. Species **1** exhibited catalytic activity toward weak acids in MeCN through a heterolytic pathway for H_2 evolution through protonation of $\text{Co}^{\text{II}}\text{-H}$ generated in situ. This suggests that the five-coordinate oxime precluded catalyst decomposition in organic media, increasing the effectiveness of the process. This feature may be relevant in the design of other ligand systems. Excellent catalytic activity was observed in water, however, this is due to the formation of nanoparticles, possibly through water incorporation into a nonconjugated imine function of **1**. This is a valuable first example of susceptibility of the molecular catalyst to its environment, and how it affects the catalytic mechanisms. We have identified this solvent effect and attempted to detect the correlated mechanisms as a means of preventing degradation.

Keywords: cobalt complexes · nanoparticles · oxime ligands · water reduction

How to cite: *Angew. Chem. Int. Ed.* **2015**, *54*, 7139–7143
Angew. Chem. **2015**, *127*, 7245–7249

[1] a) J. A. Turner, *Science* **2004**, *305*, 972–974; b) N. S. Lewis, D. G. Nocera, *Proc. Natl. Acad. Sci. USA* **2006**, *103*, 15729–15735.

- [2] a) P. Connolly, J. H. Espenson, *Inorg. Chem.* **1986**, *25*, 2684–2688; b) M. Razavet, V. Artero, M. Fontecave, *Inorg. Chem.* **2005**, *44*, 4786–4795; c) H. Xile, B. S. Brunschwig, J. C. Peters, *J. Am. Chem. Soc.* **2007**, *129*, 8988–8998; d) A. Bhattacharjee, E. S. Andreiadis, M. C. Kerlidou, M. Fontecave, M. J. Field, V. Artero, *Chem. Eur. J.* **2013**, *19*, 15166–15174.
- [3] a) S. Shi, L. M. Daniels, J. H. Espenson, *Inorg. Chem.* **1991**, *30*, 3407–3410; b) T. J. R. Weakley, J. Marks, R. G. Finke, *Acta Crystallogr. Sect. C* **1994**, *50*, 1690–1692.
- [4] a) A. Gerli, L. G. Marzilli, *Inorg. Chem.* **1992**, *31*, 1152–1160; b) K. L. Mulfort, D. M. Tiede, *J. Phys. Chem. B* **2010**, *114*, 14572–14581.
- [5] E. Anxolabéhère-Mallart, C. Costentin, M. Fournier, S. Nowak, M. Robert, J.-M. Savéant, *J. Am. Chem. Soc.* **2012**, *134*, 6104–6107.
- [6] S. E. Ghachtouli, R. Guillot, F. Brisset, A. Aukauloo, *ChemSusChem* **2013**, *6*, 2226–2230.
- [7] a) W. M. Singh, T. Baine, S. Kudo, S. Tian, X. A. N. Ma, H. Zhou, N. J. DeYonker, T. C. Pham, J. C. Bollinger, D. L. Baker, B. Yan, C. E. Webster, X. Zhao, *Angew. Chem. Int. Ed.* **2012**, *51*, 5941–5944; *Angew. Chem.* **2012**, *124*, 6043–6046; b) P. Zhang, M. Wang, F. Gloaguen, L. Chen, F. Quentel, L. Sun, *Chem. Commun.* **2013**, *49*, 9455–9457; c) L. Tong, R. Zong, R. P. Thummel, *J. Am. Chem. Soc.* **2014**, *136*, 4881–4884.
- [8] a) J. P. Bigi, T. E. Hanna, W. H. Harman, A. Chang, C. J. Chang, *Chem. Commun.* **2010**, *46*, 958–960; b) Y. Sun, J. P. Bigi, N. A. Piro, M. L. Tang, J. R. Long, C. J. Chang, *J. Am. Chem. Soc.* **2011**, *133*, 9212–9215.
- [9] a) B. D. Stubbert, J. C. Peters, H. B. Gray, *J. Am. Chem. Soc.* **2011**, *133*, 18070–18073; b) C. F. Leung, Y. Z. Chen, H. Q. Yu, S. M. Yiu, C. C. Ko, T. C. Lau, *Int. J. Hydrogen Energy* **2011**, *36*, 11640–11645.
- [10] a) M. M. Allard, F. R. Xavier, M. J. Heeg, H. B. Schlegel, C. N. Verani, *Eur. J. Inorg. Chem.* **2012**, 4622–4631; b) D. Basu, M. M. Allard, F. R. Xavier, M. J. Heeg, H. B. Schlegel, C. N. Verani, *Dalton Trans.* **2015**, *44*, 3454–3466.
- [11] D. Basu, S. Mazumder, X. Shi, H. Baydoun, J. Niklas, O. Poluektov, H. B. Schlegel, C. N. Verani, *Angew. Chem. Int. Ed.* **2015**, *54*, 2105–2110; *Angew. Chem.* **2015**, *127*, 2133–2138.
- [12] a) K. Serbest, S. Karabokek, I. Degirmencioglu, S. Guner, F. Kormali, *Transition Met. Chem.* **2001**, *26*, 375–379; b) I. C. Szigyártó, L. I. Simándi, L. Párkányi, L. Korecz, G. Schlosser, *Inorg. Chem.* **2006**, *45*, 7480–7487; c) T. Megyes, Z. May, G. Schubert, T. Grosz, L. I. Simándi, T. Radnai, *Inorg. Chim. Acta* **2006**, *359*, 2329–2336.
- [13] V. Fourmond, P. A. Jacques, M. Fontecave, V. Artero, *Inorg. Chem.* **2010**, *49*, 10338–10347.
- [14] J. T. Muckermann, E. Fujita, *Chem. Commun.* **2011**, *47*, 12456–12458.
- [15] D. Hong, J. Jung, J. Park, Y. Yamada, T. Suenobu, Y.-M. Lee, W. Nam, S. Fukuzumi, *Energy Environ. Sci.* **2012**, *5*, 7606–7616.
- [16] S. Cobo, J. Heidkamp, P.-A. Jacques, J. Fize, V. Fourmond, L. Guetaz, B. Jousselme, V. Ivanova, H. Dau, S. Palacin, M. Fontecave, V. Artero, *Nat. Mater.* **2012**, *11*, 802–807.

Received: February 17, 2015

Revised: March 26, 2015

Published online: April 27, 2015